

Orbital order in FeSe – the case for vertex renormalization

Rui-Qi Xing¹, Laura Classen² and Andrey V. Chubukov¹

¹ *School of Physics and Astronomy, University of Minnesota, Minneapolis, MN 55455, USA*

² *Condensed Matter Physics and Materials Science Department, Brookhaven National Laboratory, Upton, NY 11973-5000, USA*

We study the structure of the d-wave orbital order in FeSe in light of recent STM and ARPES data, which detect the shapes of hole and electron pockets in the nematic phase. The geometry of the pockets indicates that the sign of the orbital order $\Gamma = \langle d_{xz}^\dagger d_{xz} - d_{yz}^\dagger d_{yz} \rangle$ is different between hole and electron pockets (Γ_h and Γ_e). We argue that this sign change cannot be reproduced if one solves for the orbital order within mean-field approximation, as the mean-field analysis yields either no orbital order, or order with the same sign of Γ_e and Γ_h . We argue that another solution with the opposite signs of Γ_e and Γ_h emerges if we include the renormalizations of the vertices in d -wave orbital channel. We show that the ratio $|\Gamma_e/\Gamma_h|$ is of order one, independent on the strength of the interaction. We also compute the temperature variation of the energy of d_{xz} and d_{yz} orbitals at the center of electron pockets and compare the results with ARPES data.

Introduction Orbital degrees of freedom turned out to play an important role for iron-based superconductors (FeSC). Studies of SDW magnetism and superconductivity in these materials found that the orbital composition of the states near the Fermi surface (FS) affects the structure of the fermionic spectrum in the spin-density-wave (SDW) phase [1] and the anisotropy of the superconducting gap [2–4]. Another example where different orbitals come into play is the tetragonal-to-orthorhombic phase transition observed in many FeSCs at $T = T_s$. Below T_s , the system spontaneously breaks C_4 lattice rotational symmetry down to C_2 . This is similar to what happens in nematic liquid crystals, and, by analogy, the state below T_s is called nematic. Below T_s the occupation of d_{xz} and d_{yz} orbitals becomes unequal, i.e., the system develops an orbital order $\Gamma(|\mathbf{k}|) \propto \int d\theta_k (n_{xz}(\mathbf{k}) - n_{yz}(\mathbf{k}))$, where n_i is the density of orbital i and the integration is over the directions of \mathbf{k} for a given $|\mathbf{k}|$. Above T_s , Γ_k vanishes by C_4 symmetry, but once C_4 symmetry is broken, by one reason or the other [5], $\Gamma(|\mathbf{k}|)$ becomes finite.

In most FeSCs the range of nematic order is quite narrow as the system develops a stripe magnetic order almost immediately after the nematic order sets in. However, in FeSe (and in doped FeSe_{1-x}S_x) the regions of nematic and magnetic order are well separated in x ([6, 7])

In pure FeSe, the nematic order sets in at $T_s \approx 85K$, and magnetic order does not develop down to $T = 0$. This opens up an opportunity to extract the information about the structure of Γ from the analysis of the feedback effects on the electronic structure. The magnitude of Γ , extracted from ARPES, is $10 - 20meV$, much smaller than the fermionic bandwidth (see Refs [6, 8–15] and the discussion below). In this case, the most relevant feedback from Γ on the electrons is for momentum components in the XY plane near $k_x = k_y = 0$ and $k_x = k_y = \pi$, where hole and electron pockets are located in the 2Fe Brillouin zone (2FeBZ). The pockets in FeSe are quite small, and $\Gamma(|\mathbf{k}|)$ near these pockets is well approximated by $\Gamma(0) = \Gamma_h$ and $\Gamma(|\pi|) = \Gamma_e$.

Manifestations of the orbital order in FeSe have been seen in Raman, STM, ARPES, and other experiments

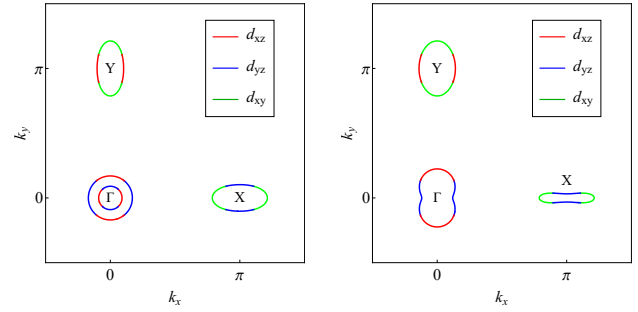


FIG. 1: The Fermi surfaces in the 1Fe BZ with the leading orbital content encoded in color. The six ψ fields, marked in the figure, are introduced in Table 1. Left panel – the FSs in the tetragonal phase, right panel – the FSs in the nematic phase. The smaller hole pocket shrinks by orbital order and completely disappears once one includes spin-orbit coupling. In FeSe, the size of the larger hole pocket depends on k_z and is the largest at $k_z = \pi$ (Ref. [16]). The parameters of the quadratic Hamiltonian used to obtain the Fermi surface are from Ref.[17]. The pockets are homogeneously enlarged to provide a better view.

(see Ref. [6] for recent review on FeSe). STM data analysis within a single domain resolved one elliptical hole Fermi surface (FS) and one electron FS, whose form becomes peanut-like below T_s (Ref. [8]). In the 1FeBZ, where electron pockets are centered at $(0, \pi)$ and $(\pi, 0)$, the observed hole pocket is elongated towards $(0, \pi)$, and the observed electron pocket is centered at $(\pi, 0)$, and its smaller axis is along the Y direction (see Fig. 1b). ARPES data on single-domain samples [9–12] show the same shape of the FSs. In multi-domain samples, ARPES shows the combination of FSs from different domains [16]. In the tetragonal phase above T_s , hole pockets are C_4 symmetric and electron pockets are elliptical (Fig. 1a). The changes from a C_4 -symmetric to an elliptical shape for the hole pocket and from an elliptical to a peanut-like shape for the $(\pi, 0)$ electron pocket are due to orbital order. Adding Γ_h and Γ_e terms to the hopping Hamiltonian in orbital representation and transforming from orbital to

band basis, one obtains [8, 17] that the observed shapes of the pockets are reproduced if $\Gamma_h > 0$ and $\Gamma_e < 0$, i.e., the orbital order changes sign between hole and electron pockets.

In this communication we address the issue how the sign change between Γ_e and Γ_h can be understood theoretically. For this, we derive and analyze the self-consistent equation for d-wave orbital order Γ . We argue that at mean-field level, the set of coupled equations for Γ_h and Γ_e contains the single effective interaction $U_0 = 5J - U$, where U and J are Hubbard and Hund local interactions. The orbital order either does not develop, when $U_0 > 0$, or does develop, if $U_0 < 0$ and its magnitude is strong enough, but the solution necessarily yields equal sign of Γ_e and Γ_h (d^{++} channel). We next include into the analysis the fact that the couplings flow away from their bare values (used in mean-field analysis), when we progressively integrate out contributions of fermions with higher energies. This flow is captured within parquet renormalization group analysis (pRG) [18] or functional RG [19]. The pRG flow splits U_0 into two different interactions U_a and U_b . We show that this splitting gives rise to a non-zero coupling in another channel for orbital ordering, this time with Γ_e and Γ_h of opposite signs (d^{+-} channel). This is similar to how the coupling in the s^{+-} pairing channel emerges due to small inter-pocket pairing interaction on top of strong Hubbard repulsion. We show that the coupling in this new orbital channel is attractive, regardless of the sign of the bare U_0 , and exceeds the coupling in the d^{++} channel. Our results are summarized in Figs. 3, 4.

Our approach is similar to earlier works [4, 20], which also found an attraction in the d^{+-} channel, but differs in detail. The authors of [4] analyzed self-consistent equations for Γ_h and Γ_e in the C_4 symmetric regime using the values of the interactions U_a and U_b near the fixed trajectory, i.e., at the very end of the pRG flow. Here we consider the evolution of U_a and U_b without assuming closeness to a fixed trajectory. This is a more realistic approach, given that in practice pRG only runs over a finite window of energies. We show that the d^{+-} channel becomes attractive from the very beginning of the pRG flow. The authors of [20] considered the case of large U/J and obtained sign-changing d^{+-} orbital order by selecting a particular combination of RPA and Aslamazov-Larkin type diagrams for the renormalization of the Hubbard interaction. We consider arbitrary U/J and treat vertex renormalizations within pRG, which accounts on equal footing for vertex renormalizations in particle-hole and particle-particle channels. Another explanation for the sign change between Γ_e and Γ_h has been put forward in Ref. [21]. It is based on the earlier study [22], which showed that the self-energy due to spin fluctuation exchange has opposite sign near Γ and near X/Y , and shrinks both hole and electron pockets. The authors of [21] argued (on a semi-phenomenological level) that the X/Y anisotropy of spin fluctuations below T_s leads to $\text{sgn}(\Gamma_e) = -\text{sgn}(\Gamma_h)$. Our approach is com-

plementary to that work: the authors of [21] included the X/Y anisotropy of the effective interaction but not orbital order. We, on the contrary, include orbital order into fermionic propagators, but neglect nematicity-induced changes of the interactions. We emphasize that both approaches lead to the sign change of the nematic splitting.

We also consider how orbital order affects the energies of d_{xz} and d_{yz} orbitals E_{xz} and E_{yz} at $(0, \pi)$ and $(\pi, 0)$ points in the 1FeBZ (the M point in the 2FeBZ). In absence of orbital order, the two energies are degenerate even in the presence of spin-orbit coupling [23]. A non-zero Γ_e breaks the degeneracy. To first order in Γ_e , the energies split – E_{xz} increases by $\Gamma_e/2$ and E_{yz} decreases by $\Gamma_e/2$. Observation of this splitting has been reported by Fedorov et al [13]. However, this group argued that the d_{xz}/d_{yz} splitting appears on top of a larger effect – a simultaneous change of the temperature dependence of E_{xz} and E_{yz} below T_s . According to Refs. [13, 16], both energies become smaller in magnitude. This observation is consistent with the later result by the same group [16] that they can resolve both electron pockets within a single domain, and both pockets have peanut-like form. A simultaneous change of the temperature dependence of E_{xz} and E_{yz} below T_s has also been reported in [14]. Later, however, Watson et al. argued [10] that they can only observe d_{yz} orbital at the M point (in addition to d_{xy}). If this is the case, then the observed T dependence below T_s can be due to the expected first-order correction in Γ_e . To address this issue, we computed the corrections to E_{xz} and E_{yz} to second order in Γ_e and Γ_h . The Γ_e^2 and Γ_h^2 terms are the same for E_{xz} and E_{yz} and, if these terms are large, they can overtake the $\pm\Gamma_e/2$ splitting already at small Γ_i . We found that the second order contribution accounts only for a small correction to $\pm\Gamma_e/2$ and, moreover, the correction is of the wrong sign. If both E_{xz} and E_{yz} indeed become smaller in magnitude below T_s , as the authors of Refs [13, 16] argue, this is due to some other physics than the one we consider here.

ψ_i	Pocket	Orbital	ψ_i	Pocket	Orbital	ψ_i	Pocket	Orbital
ψ_1	Y	d_{xz}	ψ_3	X	d_{yz}	ψ_5	Γ	d_{yz}
ψ_2	Y	d_{xy}	ψ_4	X	d_{xy}	ψ_6	Γ	d_{xz}

TABLE I: Affiliation of ψ_i with a pocket and an orbital.

Mean-field analysis We consider a model with two hole pocket near $(0, 0)$ in the tetragonal phase (H-pockets) and two electron pockets near $(0, \pi)$ and $(\pi, 0)$ in the 1FeBZ (Y and X pockets). The hole pockets are made out of d_{xz} and d_{yz} orbitals, the X pocket is made out of d_{yz} and d_{xy} orbitals and the Y pocket is made out of d_{xz} and d_{yz} (Refs. [2, 24]). We introduce six species of fermions: ψ_1, \dots, ψ_6 , see Tab I and two d -wave d_{xz}/d_{yz} orbital order parameters $\Gamma_h = \langle \psi_6^\dagger \psi_6 - \psi_5^\dagger \psi_5 \rangle$ and $\Gamma_e = \langle \psi_1^\dagger \psi_1 - \psi_3^\dagger \psi_3 \rangle$. For simplicity, we neglect d -wave orbital order on the d_{xy} orbital (the $\psi_2^\dagger \psi_2 - \psi_4^\dagger \psi_4$

term, Refs. [23, 25]). At the mean-field level, the self-consistent equations for Γ_h and Γ_e are obtained by adding up Hartree and Fock diagrams for different orbitals (Fig. 2a). To first order in the orbital order parameter, the self-energies are $\Sigma_{xz}^H = \Sigma_{h,0} + \Gamma_h/2$, $\Sigma_{yz}^H = \Sigma_{h,0} - \Gamma_h/2$, $\Sigma_{xz}^Y = \Sigma_{e,0} + \Gamma_e/2$, $\Sigma_{yz}^X = \Sigma_{e,0} - \Gamma_e/2$, where $\Sigma_{h,0}$ and $\Sigma_{e,0}$ are the self-energies in the absence of orbital order. Evaluating the diagrams and taking the difference $\Sigma_{xz}^H - \Sigma_{yz}^H = \Gamma_h$, $\Sigma_{xz}^Y - \Sigma_{yz}^X = \Gamma_e$, we obtain self-consistent equations for Γ_h, Γ_e in the form [26]

$$\begin{aligned}\Gamma_h &= U_a (n_{xz}^H - n_{yz}^H) + U_b (n_{xz}^Y - n_{yz}^X) \\ \Gamma_e &= U_a (n_{xz}^Y - n_{yz}^X) + U_b (n_{xz}^H - n_{yz}^H)\end{aligned}\quad (1)$$

Here each density n_i is the momentum integral over the corresponding Fermi function. We find, to leading order in Γ_i , $n_{xz}^H - n_{yz}^H = A_h \Gamma_h$ and $n_{xz}^Y - n_{yz}^X = A_e \Gamma_e$. To obtain the prefactors A_h and A_e , we used the orbitally-resolved low-energy model from Ref. [24] for the kinetic energy, converted from orbital to band basis, and computed the momentum integrals of the Fermi functions for different bands, weighted by the "coherent" factors associated with the change of the basis. We present the details of the calculations in [27] and here state the result: both A_h and A_e are negative, and their ratio $\gamma = A_e/A_h$ depends on the parameters in the kinetic energy and is, in general, of order one. Using the band structure parameters that fit the ARPES and STM data, we obtained $\gamma \sim 0.2$ (see [27]).

The interactions U_a and U_b are linear combinations of seven different interactions involving d_{xz} and d_{yz} orbital states near momenta where FSs are located. We show these seven interactions in Fig. 2b. In terms of these interactions, $U_a = U_5 - 2\tilde{U}_5 + \bar{U}_5$ [28] and $U_b = 2(U_1 - \bar{U}_1) - (U_2 - \bar{U}_2)$ (labels are as in Fig. 2b). The bare values of the seven couplings are $U_5^{(0)} = U_1^{(0)} = U_2^{(0)} = U$, $\tilde{U}_5^{(0)} = \bar{U}_1^{(0)} = U'$, $\tilde{U}_5^{(0)} = \bar{U}_2^{(0)} = J$. As a result, the bare $U_a^{(0)}$ and $U_b^{(0)}$ are the same: $U_a^{(0)} = U_b^{(0)} = U_0 = U + J - 2U'$. If we take $U' = U - 2J$ (Ref. [2]), we obtain $U_0 = 5J - U$. Substituting $U_a = U_b = U_0$ into (1), we obtain that the only possible solution of the self-consistent set is $\Gamma_h = \Gamma_e$ (sign-preserving d^{++} orbital order), and this order develops if the eigenvalue $\lambda^{++} = U_0(A_h + A_e) > 1$. The solution with the opposite sign of Γ_e and Γ_h does not emerge at the mean-field level.

Beyond mean-field We now go beyond mean-field and include into consideration that the seven interactions, which contribute to U_a and U_b , flow to different values as one progressively integrates out fermions with higher energies. This flow can be captured within pRG and comes from mutual vertex renormalizations of the total of 30 different interactions between low-energy fermions on d_{xz}, d_{yz} , and d_{xy} orbitals [4, 24, 25]. The flow equations have been derived in [25], and we use the results of that work to obtain the flow of U_a and U_b . The results are shown in Fig. 3. We see that U_a and U_b become different from U_0 , and $U_b > U_a$, irrespective of

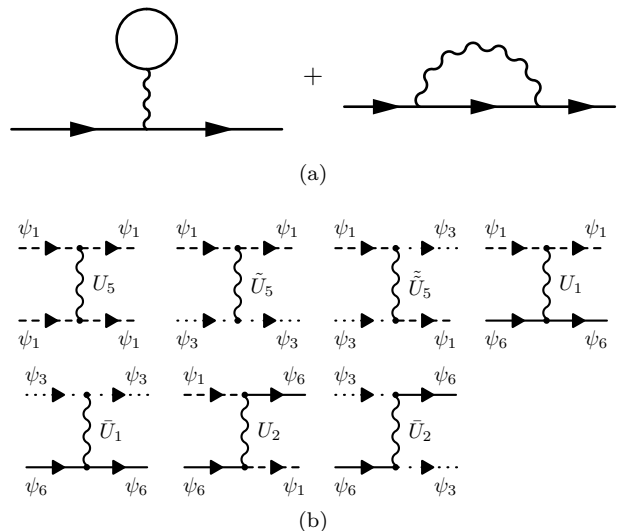


FIG. 2: a) Hartree and Fock self-energy diagrams; b) Examples of the interaction terms which contribute to Hartree-Fock self-energies. The U_5 terms in the first row also act on hole pockets (ψ_5, ψ_6). Each diagram has symmetry-equivalents. ($\psi_1 \leftrightarrow \psi_3$, $\psi_5 \leftrightarrow \psi_6$). The self-energy beyond mean-field has been computed using dressed interactions, which we obtained using pRG scheme. In a direct perturbation theory, this amounts to summing up infinite series of self-energy diagrams, including RPA and Aslamazov-Larkin diagrams.

whether $U_0 > 0$ or $U_0 < 0$. Solving for the eigenfunctions and eigenvalues of Eq. (1) when U_a and U_b are different, we obtain an eigenfunction $\Gamma^{++} = \Gamma_h + \alpha_+ \Gamma_e$ with the eigenvalue λ^{++} and $\Gamma^{+-} = \Gamma_h + \alpha_- \Gamma_e$ with the eigenvalue λ^{+-} , where

$$\begin{aligned}\alpha_{\pm} &= -\frac{1-\gamma}{2} \frac{U_a}{U_b} \pm \sqrt{\left(\frac{1-\gamma}{2}\right)^2 \frac{U_a^2}{U_b^2} + \gamma} \\ \lambda^{+,+} &= -|A_h| \left[\frac{1+\gamma}{2} U_a \pm U_b \sqrt{\left(\frac{1-\gamma}{2}\right)^2 \frac{U_a^2}{U_b^2} + \gamma} \right]\end{aligned}\quad (2)$$

We see that $\alpha_+ > 0$ and $\alpha_- < 0$, i.e., the eigenfunction Γ^{++} describes sign-preserving d^{++} orbital order and Γ^{+-} describes sign-changing d^{+-} order. We plot the corresponding eigenvalues λ^{++} and λ^{+-} in Fig. 4. We see that λ^{+-} becomes positive (i.e., attractive) for any sign of U_0 , once we include the pRG flow of the interactions. We emphasize that this holds even if the flow runs only over a small range of energies. For an instability towards a sign-changing orbital order, the flow needs to run over a finite range of energies to reach $\lambda^{+-} > 1$.

For $U_0 > 0$, the coupling in the λ^{++} channel is repulsive, i.e., d^{+-} orbital order is the only solution of Eq. (1). For $U_0 < 0$, the d^{++} channel is attractive at the bare level, but we see from Fig. 4c,d that it becomes sub-leading once U_b changes sign under pRG (see Fig. 3b). The attraction in d^{+-} orbital channel for $U_0 < 0$ was earlier obtained in Ref. [20] who used a combina-

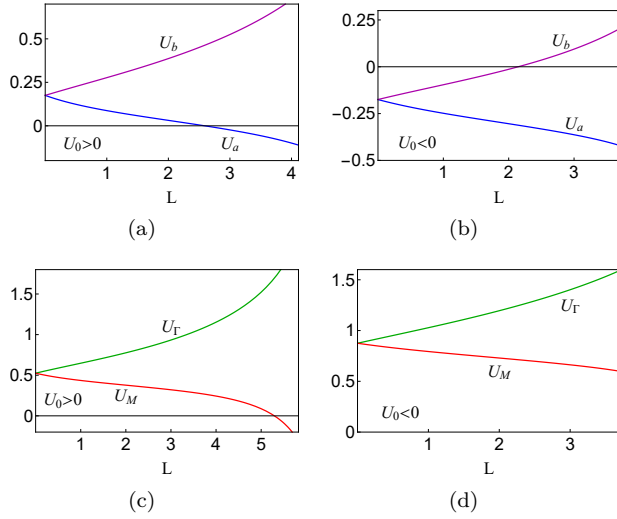


FIG. 3: Panels (a) and (b) – the pRG flow of the couplings U_a and U_b for the case when the bare $U_a^{(0)} = U_b^{(0)} = U_0 = 5J - U$ is positive in (a) and negative in (b) (we set $J/U = 0.3$ and 0.1 , respectively). Panels (c) and (d) – the flow of the couplings U_M and U_Γ in Eq. (3). The parameter $L = \log \frac{W}{E}$, where W is of order bandwidth and E is the running energy. The larger L is, the more high energy states are integrated out. We used $m_h U / (4\pi) = 0.35$ where m_h is the mass of the dispersion near the hole pocket.

tion of RPA spin and charge channels and Aslamazov-Larkin diagrams to separate U_a and U_b . In distinction with Ref. [20], here we account for the renormalization of U_a and U_b systematically, in an order-by-order treatment (as pRG is), through all channels including the pairing channel. Like we said, we found that λ^{+-} becomes positive already at the very beginning of the pRG flow, when the renormalization of $U_{a,b}$ can be obtained within a direct perturbative expansion. In particular, the condition $U_0 < 0$ is not required [29]. We note in this regard that our computation of the self-energy, using the diagrams in Fig. 2a with the dressed interactions obtained within the pRG scheme, is diagrammatically equivalent to summing up infinite series of contributions to the self-energy, including both RPA and Aslamazov-Larkin diagrams.

Temperature variations of E_{xz} and E_{yz} . We now analyze how the energies E_{xz} at $(0, \pi)$ and E_{yz} at $(\pi, 0)$ vary with increasing orbital order (in the 2FBZ these are energies of d_{xz}/d_{yz} orbitals at M). To first order in Γ_e , the two energies just split: $E_{xz} = E_{e,0} + \Gamma_e/2$ and $E_{yz} = E_{e,0} - \Gamma_e/2$, where $E_{e,0} < 0$ is the energy in the absence of the nematic order [23, 24]. Our goal is to go beyond the first order in Γ_e and check if there is a large common term of order $\Gamma_{e,h}^2$. A large positive $\Gamma_{e,h}^2$ term would be consistent with Refs. [13, 16]. The authors of these papers argued, based on interpretation of their ARPES data, that the magnitude of both E_{xz} and E_{yz} are reduced in the nematic phase.

To check this possibility, we computed the self-energies Σ_{xz}^Y and Σ_{yz}^X to order Γ^2 . We did not do the full self-

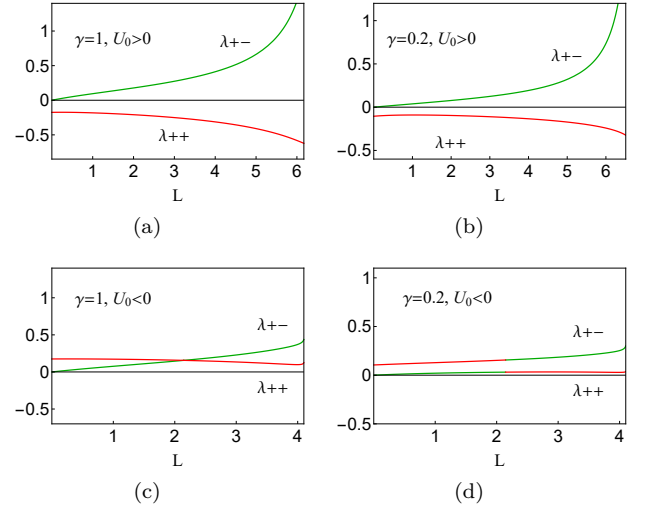


FIG. 4: The flow of the dimensionless couplings λ^{++} in sign-preserving d^{++} channel (green) and λ^{+-} in sign-changing d^{+-} channel (red). Notations are as in Fig. 3. Panels (a) and (b) – the flow for the case $U_0 = 5J - U > 0$ for two values of the parameter $\gamma = A_e/A_h$ (see text). Panels (c) and (d) – the same for $U_0 < 0$. The sign-changing d^{+-} channel becomes dominant once U_b changes sign near $L = 2$. For $\gamma \neq 1$, the couplings jump by finite values when U_b passes through zero.

consistent calculation to this order, as it would require to include the self-energy to order Γ^2 into the densities $n_{xz}^H, n_{yz}^H, n_{xz}^Y$, and n_{yz}^X . Rather, we evaluated the "source" term in the self-energy $\Sigma_{so}(\Gamma)$, which comes from keeping $O(\Gamma_{h,e})$ terms in the self-energy, but expanding the densities to order $\Gamma_{h,e}^2$. The common self-energy for Σ_{xz}^Y and Σ_{yz}^X below the nematic transition is proportional to $\Sigma_{so}(\Gamma) - \Sigma_{so}(0)$. We find

$$\Sigma_{so}(\Gamma) = U_M(n_{xz}^Y + n_{yz}^X) + U_\Gamma(n_{xz}^H + n_{yz}^H) \quad (3)$$

and $U_M = U_5 + 2\tilde{U}_5 - \tilde{\tilde{U}}_5$ and $U_\Gamma = 2(U_1 + \bar{U}_1) - (U_2 + \bar{U}_2)$. The bare value of U_M and U_Γ are again equal, each is $U + 2U' - J$ ($= 3U - 5J$ if $U' = U - 2J$), but under pRG, U_Γ becomes larger than U_M , as we show in Fig. 3 c,d. The common densities are $(n_{xz}^H + n_{yz}^H) = n_{h,0} + B_h \Gamma_h^2$, $(n_{xz}^Y + n_{yz}^X) = n_{e,0} + B_e \Gamma_e^2$, where $n_{i,0}$ labels the density for $\Gamma_i = 0$. We find (see [27] for details) $B_h < 0$ and $|B_e| \leq |B_h|$. In this situation, the common correction to E_{xz}^Y and E_{yz}^X is negative. Given that $E_{e,0}$ is also negative, we see the common self-energy makes the two energies more negative. Furthermore, the magnitude of B_h is at most of order $1/T_s$, hence near T_s , when $\Gamma_{h,e}$ are small, the self-energy to second order in Γ_i is a small correction to the first-order $\pm \Gamma_i/2$ term. This is inconsistent with the interpretation of the data in Refs. [13, 16].

Conclusions. In this communication we presented the solution of self-consistent equations for d-wave nematic order parameters on d_{xz}/d_{yz} orbitals. We argued that at a mean-field level the only solution possible is sign-preserving d^{++} nematic order Γ (same sign of Γ_e

and Γ_h) when the bare coupling $U_0 < 0$. We went beyond mean-field and included the flow of the couplings under pRG. Then we found an attraction in d^{+-} channel for which Γ_e and Γ_h have opposite sign, in agreement with STM and ARPES data. We argued that d^{+-} orbital order becomes the leading instability for either sign of bare U_0 . We also computed the common self-energy for d_{xz} and d_{yz} orbitals at the center of electron pockets to second order in Γ to check whether we can reproduce the results of Refs. [13, 16] that the energies E_{xz}^Y and E_{yz}^X simultaneously get smaller by magnitude in the nematic phase. We obtained a much smaller self-energy and of opposite sign than the one which is needed. If the interpretation of the data in [13, 16] is correct, it has to be due to a self-energy with vertices beyond our RG analysis.

Acknowledgments. We thank A. Coldea, L. Bas-

conses, L. Benfatto, S. Borisenko, D. Chichinadze, R.M. Fernandes, J. Kang, T.K. Kim, W. Ku, L. de' Medici, M. Watson, and Y.M. Wu for useful discussions. R.X. and A.V.C. are supported by the Office of Basic Energy Sciences, U.S. Department of Energy, under award DE-SC0014402. L.C. acknowledges support from the Alexander-von-Humboldt foundation. Work at BNL is supported by the U.S. Department of Energy (DOE), Division of Condensed Matter Physics and Materials Science, under Contract No. DE-SC0012704. Part of the work was done while A.V.C. was visiting KITP in Santa Barbara. KITP is supported by NSF under Grant No. NSF PHY17-48958. RX and LC equally contributed to this project.

Supplemental Material

Orbital order in FeSe – the case for vertex renormalization

I. ORBITALLY-RESOLVED LOW-ENERGY MODEL

We use an effective orbitally-resolved, low-energy model to describe excitations near the Fermi pockets in FeSe. The model can be constructed by expanding the hopping integrals near the centers of hole and electron pockets [24]. We will work in the "theoretical" 1FeBZ, where the hole pockets are centered at $\Gamma = (0, 0)$, and the electron pockets are centered at $X = (\pi, 0)$ and $Y = (0, \pi)$. The two Γ -centered pockets are made out of d_{xz} and d_{yz} orbitals, the X pocket is made out of d_{yz} and d_{xy} orbitals and the Y pocket is made out of d_{xz} and d_{xy} (Refs. [2, 24]), as shown in Fig. 1. The dispersion in the physical 2FeBZ can be obtained by folding the 1FeBZ along its diagonal. Under the folding, the points Y and X both become $M = (\pi, \pi)$.

We introduce six species of fermions: ψ_1, \dots, ψ_6 . Fermions ψ_1 and ψ_2 describe d_{xz} and d_{xy} excitations near the electron pocket at Y, ψ_3 and ψ_4 describe d_{yz} and d_{xy} excitations near the X pocket, and ψ_5 and ψ_6 describe d_{xz} and d_{yz} excitations near the hole pockets at Γ . The assignment is summarized in Tab I and sketched in Fig. 1.

The quadratic Hamiltonian for states close to the hole pocket is

$$H^\Gamma = \sum_{\mathbf{k}, \sigma} \left(\psi_{5\sigma}^\dagger(\mathbf{k}), \psi_{6\sigma}^\dagger(\mathbf{k}) \right) h_\Gamma(\mathbf{k}) \begin{pmatrix} \psi_{5\sigma}(\mathbf{k}) \\ \psi_{6\sigma}(\mathbf{k}) \end{pmatrix} \quad (S1)$$

with

$$h_\Gamma(\mathbf{k}) = \begin{pmatrix} \epsilon_h - \frac{k^2}{2m_h} + \frac{b}{2}(k_x^2 - k_y^2) - \Gamma_h & ck_x k_y \\ ck_x k_y & \epsilon_h - \frac{k^2}{2m_h} - \frac{b}{2}(k_x^2 - k_y^2) + \Gamma_h \end{pmatrix}, \quad (S2)$$

In the tetragonal phase, $\Gamma_h = 0$. In the orthorhombic phase at $T < T_s$, Γ_h has a finite value.

To make the formulas more compact, we assume $b = c$. Then in the tetragonal phase the hole pockets are circular, with energies $\epsilon_{c,d}^{tet} = \epsilon_h - (k^2/(2m_h))(1 \pm bm_h)$. The band operators c_k and d_k of the inner and outer hole pocket are related to $\psi_5(k)$ and $\psi_6(k)$ by a rotation

$$c_k = -\sin \theta_\Gamma(k) \psi_5(k) + \cos \theta_\Gamma(k) \psi_6(k), \quad d_k = \cos \theta_\Gamma(k) \psi_5(k) + \sin \theta_\Gamma(k) \psi_6(k) \quad (S3)$$

where $\theta_\Gamma(k)$ corresponds to the polar angle along a hole pocket, counted from the k_x -axis.

In the orthorhombic (nematic) phase, the dispersion of hole-like excitations is altered to

$$\epsilon_{c,d}^{nem} = \epsilon_h - k^2/(2m_h) \mp \sqrt{b^2 k^4 + 4\Gamma_h^2 - 4bk\Gamma_h \cos \theta}. \quad (S4)$$

The transformation to band basis can still be viewed as a rotation, like in Eq. (S3), but the rotation angle $\phi_\Gamma(k)$ no longer coincides with $\theta_\Gamma(k)$ and is expressed as [5, 17]

$$\tan \phi_\Gamma(k) = \frac{\sin 2\theta_\Gamma(k)}{\cos 2\theta_\Gamma(k) - 2\Gamma_h/(bk^2)} \quad (\text{S5})$$

The excitations near the electron pockets are described by

$$H^{Y,X} = \sum_{\mathbf{k},\sigma} \left(\psi_{1,3\sigma}^\dagger(\mathbf{k}), \psi_{2,4\sigma}^\dagger(\mathbf{k}) \right) h_{Y,X}(\mathbf{k}) \begin{pmatrix} \psi_{1,3\sigma}(\mathbf{k}) \\ \psi_{2,4\sigma}(\mathbf{k}) \end{pmatrix} \quad (\text{S6})$$

with

$$h_{Y,X}(\mathbf{k}) = \begin{pmatrix} \epsilon_1 + \frac{k^2}{2m_1} \pm \frac{a_1}{2}(k_x^2 - k_y^2) \pm \Gamma_e & -\sqrt{2}ivk_{x/y} \\ \sqrt{2}ivk_{x/y} & \epsilon_2 + \frac{k^2}{2m_2} \pm \frac{a_2}{2}(k_x^2 - k_y^2) \end{pmatrix} \quad (\text{S7})$$

where the upper sign is for the Y pocket and the lower for the X pocket. In the tetragonal phase $\Gamma_e = 0$, in the orthorhombic phase it is finite. The parameters $v, \epsilon_{1,2}, a_{1,2}$, and $m_{1,2}$ can be determined by fitting the band structure to ARPES data. For FeSe they are given in the supplemental of Ref. [17]. In the band basis, this gives two branches around the X point and two branches around the Y point. Only one dispersion from each pair crosses the Fermi level and forms the electron pocket at X or Y .

In the tetragonal phase the energies of the bands that cross the Fermi level are given by $\epsilon_{X,Y}^{tet} = \frac{1}{2}(C_1^{X,Y} + C_2^{X,Y}) + \frac{1}{2}\sqrt{(C_1^{X,Y} - C_2^{X,Y})^2 + 8v^2k_{y,x}^2}$ with $C_i^{X,Y} = \epsilon_i + k^2/(2m_i) \mp a_i/2(k_x^2 - k_y^2)$. The bands that do not cross the Fermi level have energies $\tilde{\epsilon}_{X,Y}^{tet} = \frac{1}{2}(C_1^{X,Y} + C_2^{X,Y}) - \frac{1}{2}\sqrt{(C_1^{X,Y} - C_2^{X,Y})^2 + 8v^2k_{y,x}^2}$. The conversion from orbital to band basis can be again written as rotation

$$e_{X,Y} = \mp i \cos \phi_{X,Y} \psi_{3,1} + \sin \phi_{X,Y} \psi_{4,2}, \quad \tilde{e}_{X,Y} = \pm i \sin \phi_{X,Y} \psi_{3,1} + \cos \phi_{X,Y} \psi_{4,2} \quad (\text{S8})$$

where e_i labels the band that forms the electron pocket and \tilde{e}_i the one that does not cross the Fermi level. However, the angle $\phi_{X,Y}$ does not coincide with the polar angle along an electron pocket. To a good approximation, $\cos \phi_{X,Y} = A \sin \theta_{X,Y}$ and $\sin \phi_{X,Y} = \sqrt{1 - A^2 \sin^2 \theta_{X,Y}}$, where $\theta_{X(Y)}$ is the polar angle measured along $\Gamma - X$ ($\Gamma - Y$) and $1/\sqrt{2} < A < 1$ is a constant [17, 25].

In the orthorhombic phase, the energies of the bands that cross the Fermi level become

$$\epsilon_{X,Y}^{nem} = \frac{1}{2}(C_1^{X,Y} + C_2^{X,Y} \mp \Gamma_e) + \frac{1}{2}\sqrt{(C_1^{X,Y} - C_2^{X,Y} \mp \Gamma_e)^2 + 8v^2k_{y,x}^2}. \quad (\text{S9})$$

The transformation from orbital to band space can still be written as in (S8), but the relations between $\phi_{X,Y}$ and $\theta_{X,Y}$ change to $\cos \phi_{X,Y} = A_{X,Y} \sin \theta_{X,Y}$ and $\sin \phi_{X,Y} = \sqrt{1 - A_{X,Y}^2 \sin^2 \theta_{X,Y}}$ with $A_{X,Y} = A(1 \mp \frac{\Gamma_e}{\Delta E}(1 - A^2 \sin^2 \theta_{X,Y}))$ and $\Delta E = \tilde{\epsilon}_X^{tet}(k_F^X)$, where k_F^X is the Fermi wave vector of the electron pocket at X (Ref. [17]). In the following, we approximate $A_{X,Y}$ by their average values along the electron FSs: $A_{X,Y} = A(1 \mp \beta \Gamma_e)$ with $\beta = (1 - A^2/2)/\Delta E$. The constant ΔE is given by $\tilde{\epsilon}_X^0(k_F^X)$, where k_F^X is the Fermi wave vector of the electron pocket at X .

There are 30 symmetry-allowed interactions between six fermion species ψ_i [24, 25]. We assume that interactions involving d_{xy} fermions are small, by one reason or the other (e.g., by applying full pRG to the full model with 30 couplings [25]), and focus on the interaction terms which involve fermions from d_{xz} and d_{yz} orbitals. These interactions are

$$\begin{aligned} H_{int} = & U_1 \sum' \left[\psi_{1\sigma}^\dagger \psi_{1\sigma} \psi_{6\sigma'}^\dagger \psi_{6\sigma'} + \psi_{3\sigma}^\dagger \psi_{3\sigma} \psi_{5\sigma'}^\dagger \psi_{5\sigma'} \right] + \bar{U}_1 \sum' \left[\psi_{1\sigma}^\dagger \psi_{1\sigma} \psi_{5\sigma'}^\dagger \psi_{5\sigma'} + \psi_{3\sigma}^\dagger \psi_{3\sigma} \psi_{6\sigma'}^\dagger \psi_{6\sigma'} \right] \\ & + U_2 \sum' \left[\psi_{1\sigma}^\dagger \psi_{6\sigma} \psi_{6\sigma'}^\dagger \psi_{1\sigma'} + \psi_{3\sigma}^\dagger \psi_{5\sigma} \psi_{5\sigma'}^\dagger \psi_{3\sigma'} \right] + \bar{U}_2 \sum' \left[\psi_{1\sigma}^\dagger \psi_{5\sigma} \psi_{5\sigma'}^\dagger \psi_{1\sigma'} + \psi_{3\sigma}^\dagger \psi_{6\sigma} \psi_{6\sigma'}^\dagger \psi_{3\sigma'} \right] \\ & + \frac{U_4}{2} \sum' \left[\psi_{5\sigma}^\dagger \psi_{5\sigma} \psi_{5\sigma'}^\dagger \psi_{5\sigma'} + \psi_{6\sigma}^\dagger \psi_{6\sigma} \psi_{6\sigma'}^\dagger \psi_{6\sigma'} \right] \\ & + \tilde{U}_4 \sum' \psi_{5\sigma}^\dagger \psi_{5\sigma} \psi_{6\sigma'}^\dagger \psi_{6\sigma'} + \tilde{U}_4 \sum' \psi_{5\sigma}^\dagger \psi_{6\sigma} \psi_{6\sigma'}^\dagger \psi_{5\sigma'} + \frac{U_5}{2} \sum' \left[\psi_{1\sigma}^\dagger \psi_{1\sigma} \psi_{1\sigma'}^\dagger \psi_{1\sigma'} + \psi_{3\sigma}^\dagger \psi_{3\sigma} \psi_{3\sigma'}^\dagger \psi_{3\sigma'} \right] \\ & + \tilde{U}_5 \sum' \psi_{1\sigma}^\dagger \psi_{1\sigma} \psi_{3\sigma'}^\dagger \psi_{3\sigma'} + \tilde{U}_5 \sum' \psi_{1\sigma}^\dagger \psi_{3\sigma} \psi_{3\sigma'}^\dagger \psi_{1\sigma'} \end{aligned}$$

(S10)

The summation is over spin components and over momenta, under the constraint of momentum conservation. These interactions describe all symmetry-allowed scattering processes between d_{xz} and d_{yz} fermions near electron and hole pockets. We omitted pair hopping terms because they do not play a role in the following.

If we use the microscopic model with local Hubbard-Hund interactions, the interaction parameters are [25]

$$\begin{aligned} U_1 &= U_2 = U_4 = U_5 = U, \\ \bar{U}_1 &= \tilde{U}_4 = \tilde{U}_5 = U', \\ \bar{U}_2 &= \tilde{U}_4 = \tilde{U}_5 = J, \end{aligned} \tag{S11}$$

II. SELF-CONSISTENT EQUATIONS FOR Γ_h AND Γ_e

To obtain the self-consistent equations for the nematic order parameters Γ_h and Γ_e , we evaluate the Hartree and Fock diagrams for the self-energies Σ_{xz} and Σ_{yz} near hole and electron pockets. In orbital basis, these self-energies contribute to the diagonal terms in Eqs. (S2) and (S7). Each self-energy contains a piece from the tetragonal phase and a piece which depends on Γ_e and Γ_h . To first order in the orbital order, $\Sigma_{xz}^\Gamma = \Sigma_{tet}^\Gamma + \Gamma_h/2$ and $\Sigma_{yz}^\Gamma = \Sigma_{tet}^\Gamma - \Gamma_h/2$, where Σ_{tet}^Γ is the self-energy at the Γ point in the tetragonal phase. At momenta close, but not equal to Γ , the self-energy acquires some k -dependence already in the tetragonal phase, but this dependence is small and irrelevant for our purposes, and we neglect it. Taking the difference between the two self-energies, we obtain $\Sigma_{xz}^\Gamma - \Sigma_{yz}^\Gamma = \Gamma_h$. Similarly, $\Sigma_{xz}^Y - \Sigma_{yz}^X = \Gamma_e$. Evaluating the diagrams for the self-energies then leads to

$$\begin{aligned} \Gamma_h &= U_{a4} (n_{xz}^\Gamma - n_{yz}^\Gamma) + U_b (n_{xz}^Y - n_{yz}^X) \\ \Gamma_e &= U_{a5} (n_{xz}^Y - n_{yz}^X) + U_b (n_{xz}^\Gamma - n_{yz}^\Gamma), \end{aligned} \tag{S12}$$

The differences $n_{xz}^\Gamma - n_{yz}^\Gamma$ and $n_{xz}^Y - n_{yz}^X$ vanish in the tetragonal phase and are proportional to Γ_h and Γ_e , respectively. Eq. (S12) then becomes a self-consistent set of linearized equations for Γ_h and Γ_e . Solving the set, one obtains T_s and the ratio Γ_e/Γ_h near T_s . We assume that the sign of Γ_e/Γ_h will not change at a smaller T , when non-linear terms in the r.h.s. of (S12) become relevant.

The interaction terms in (S12) are $U_{a5} = U_5 - 2\tilde{U}_5 + \tilde{\tilde{U}}_5$, $U_{a4} = U_4 - 2\tilde{U}_4 + \tilde{\tilde{U}}_4$ and $U_b = 2(U_1 - \bar{U}_1) - (U_2 - \bar{U}_2)$. If we use the local Hubbard-Hund model Eq. (S11), we obtain $U_{a5} = U_{a4} = U_b = U + J - 2U'$. However, the couplings become different once we include vertex corrections to U_{a5} , U_{a4} , and U_b . In the main text we present the results for the dressed couplings assuming that the running U_{a5} and U_{a4} remain equal, i.e., the running $U_{a5} = U_{a4} = U_a$. Here we present the results for a generic case when only bare $U_{a5} = U_{a4}$, but the running couplings are different. The running couplings U_{a5} and U_{a4} follow each other, and their ratio tends to constant r , whose value depends on system parameters [25]. Below we use $U_{a5} = U_a$ and $U_{a4} = rU_a$, when we will be using the dressed couplings.

The fermionic densities are the integrals over momentum and sums over Matsubara frequencies of the corresponding Green's functions: $(n_{xz}^\Gamma - n_{yz}^\Gamma) = T \sum_{\omega_m} \int d^k / (2\pi)^2 (G_{xz}^\Gamma(k, \omega_m) - G_{yz}^\Gamma(k, \omega_m))$ and $(n_{xz}^Y - n_{yz}^X) = T \sum_{\omega_m} \int d^k / (2\pi)^2 (G_{xz}^Y(k, \omega_m) - G_{yz}^X(k, \omega_m))$. To evaluate the integrals, we transfer the Green's functions to the band basis and express the result in terms of the corresponding Fermi functions. One can check that in the tetragonal phase the self-energies Γ_{tet}^Γ and $\Gamma_{tet}^{X,Y}$ come from states not confined to the FSs, however the additional terms in the orthorhombic phase, proportional to Γ_h and Γ_e , come from the states near Γ , X, or Y points. In explicit form, we obtain near hole pockets

$$\begin{aligned} (n_{xz}^\Gamma - n_{yz}^\Gamma) &= \int \frac{d^2k}{(2\pi)^2} \cos 2\phi_H \left(n_F(\epsilon_c^{nem}) - n_F(\epsilon_d^{nem}) \right) = A_h \Gamma_h \\ A_h &= - \int \frac{d^2k}{(2\pi)^2} \left[\frac{2}{bk_F^2} \sin^2 2\theta \left(n_F(\epsilon_c^{tet}) - n_F(\epsilon_d^{tet}) \right) + \frac{1}{T} \cos^2 2\theta \left(\frac{e^{\epsilon_c^{tet}/T}}{(1 + e^{\epsilon_c^{tet}/T})^2} + \frac{e^{\epsilon_d^{tet}/T}}{(1 + e^{\epsilon_d^{tet}/T})^2} \right) \right] + \mathcal{O}(\Gamma_h^2) \end{aligned} \tag{S13}$$

where n_F is the Fermi distribution function and the expressions for $\epsilon_c^{tet} = \epsilon_c^{tet}(k)$ and $\epsilon_d^{tet} = \epsilon_d^{tet}(k)$ are given above. We recall that c -operators describe the inner hole pocket and d -operators describe the outer hole pocket. Accordingly,

$\epsilon_c^{tet} \leq \epsilon_d^{tet}$, so that $n_F(\epsilon_c^{tet}) \geq n_F(\epsilon_d^{tet})$. As a result, both terms in the last line in (S13) have the same sign, hence $A_h < 0$. We used this in the main text.

Similarly, fermionic densities in the vicinity of the electron pockets are given by

$$\begin{aligned} (n_{xz}^Y - n_{yz}^X) &= \int \frac{d^2k}{(2\pi)^2} [\cos^2 \phi_Y n_F(\epsilon_Y) - \cos^2 \phi_X n_F(\epsilon_X)] \\ &= \int \frac{d^2k}{(2\pi)^2} [A^2(1 + \beta\Gamma_e)^2 \sin^2 \theta_Y n_F(\epsilon_Y^{nem}) - A^2(1 - \beta\Gamma_e)^2 \sin^2 \theta_X n_F(\epsilon_X^{nem})] = A_e \Gamma_e \\ A_e &= A^2 \int \frac{d^2k}{(2\pi)^2} \cos^2 \theta \left[2\beta n_F(\epsilon_Y^{tet}) - \frac{1}{T} f_Y(k) \frac{e^{\epsilon_Y^{tet}/T}}{(1 + e^{\epsilon_Y^{tet}/T})^2} \right] + \mathcal{O}(\Gamma_e^2). \end{aligned} \quad (\text{S14})$$

Here, the function $f_Y(k)$ is obtained when expanding the band energies to linear order in Γ_e , e.g., $\epsilon_Y^{nem} = \epsilon_Y^{tet} + f_Y(k)\Gamma_e/2$ with $f_Y(k) = 1 + (C_1^Y - C_2^Y)/\sqrt{(C_1^Y - C_2^Y)^2 + 8v^2k_x^2}$. To check the sign of A_e we evaluate the momentum integral in the last line in (S14) analytically by setting $a_{1,2} = v = 0$ in (S7). We obtain

$$A_e = A^2 \frac{m_e}{2\pi} \left(\beta|\epsilon_1| + \beta T \ln \left(1 + e^{-|\epsilon_1|/T} \right) - \frac{1}{1 + e^{-|\epsilon_1|/T}} \right) \quad (\text{S15})$$

For FeSe, $\beta|\epsilon_1| \sim 1/4$. For such β , A_e is negative. We then determine A_e numerically, using the full quadratic Hamiltonian in (S7) and the values of parameters for FeSe as given in Ref. [17]. We again obtain that A_e is negative. We used that $A_e < 0$ in the main text. The magnitudes of A_h and A_e are comparable, but A_h is larger: we found numerically $\gamma = A_e/A_h \approx 0.2$.

Using these results, we can write the self-consistent equations on Γ_h and Γ_e as

$$\begin{aligned} \Gamma_h &= -|A_h| (rU_a\Gamma_h + \gamma U_b\Gamma_e) \\ \Gamma_e &= -|A_h| (\gamma U_a\Gamma_e + U_b\Gamma_h). \end{aligned} \quad (\text{S16})$$

In the main term we presented this equation and its solution (see below) for $r = 1$.

The two eigenmodes of the set (S16) are

$$\Gamma_h + \alpha_{\pm}\Gamma_e = \lambda^{+,+}(\Gamma_h + \alpha_{\pm}\Gamma_e) \quad (\text{S17})$$

with

$$\begin{aligned} \alpha_{\pm} &= -\frac{r - \gamma}{2} \frac{U_a}{U_b} \pm \sqrt{\left(\frac{r - \gamma}{2}\right)^2 \frac{U_a^2}{U_b^2} + \gamma} \\ \lambda^{+,+} &= -|A_h| \left[\frac{r + \gamma}{2} U_a \pm U_b \sqrt{\left(\frac{r - \gamma}{2}\right)^2 \frac{U_a^2}{U_b^2} + \gamma} \right], \end{aligned} \quad (\text{S18})$$

III. COMMON PART OF THE SELF-ENERGIES TO ORDER $\Gamma_{h,e}^2$

We now show the details of the evaluation of the common part of the self-energies Σ_{xz}^Y and Σ_{yz}^X to second order in $\Gamma_{h,e}$. We can isolate the quadratic terms by evaluating $\Sigma_2 = \Sigma_{xz}^Y + \Sigma_{yz}^X - 2\Sigma^{tet}$. The common self-energy Σ_2 is given by

$$\Sigma_2 = U_M(n_{xz}^Y + n_{yz}^X) + U_{\Gamma}(n_{xz}^{\Gamma} + n_{yz}^{\Gamma}) \quad (\text{S19})$$

where $U_M = U_5 + 2\tilde{U}_5 - \tilde{\tilde{U}}_5$ and $U_{\Gamma} = 2(U_1 + \bar{U}_1) - (U_2 + \bar{U}_2)$. The sums of the densities in the vicinity of the hole pockets are

$$\begin{aligned} (n_{xz}^{\Gamma} + n_{yz}^{\Gamma}) &= \int \frac{d^2k}{(2\pi)^2} (n_F(\epsilon_c^{nem}) + n_F(\epsilon_d^{nem})) + n_{tet}^{\Gamma} \\ &= \Gamma_h^2 \int \frac{d^2k}{(2\pi)^2} \sum_{i=c,d} e^{\epsilon_i^{tet}/T} \left[\sigma_i \frac{1}{Tbk_F^2} \frac{1}{(1 + e^{\epsilon_i^{tet}/T})^2} + \frac{1}{2T^2} \cos^2 \theta \frac{e^{\epsilon_i^{tet}/T} - 1}{(1 + e^{\epsilon_i^{tet}/T})^3} \right] + n_{tet}^{\Gamma} \end{aligned}$$

$$= -\Gamma_h^2 \left[\frac{bm_h^2}{1 - b^2m_h^2} \frac{1}{2\pi bk_F^2} \left(\tanh \left(1 + \frac{\epsilon_h}{2T} \right) \right) + \frac{1}{8T \cosh^2 \frac{\epsilon_h}{2T}} \right] + n_{tet}^\Gamma \quad (\text{S20})$$

where $\sigma_i = 1(-1)$ for $i = c(d)$, ϵ_h is defined after Eq. (S2), and n_{tet}^Γ is the density around hole pockets in the tetragonal phase. We define $(n_{xz}^H + n_{yz}^H) = n_{tet}^\Gamma + B_h \Gamma_h^2$. Then

$$B_h = - \left[\frac{bm_h^2}{1 - b^2m_h^2} \frac{1}{2\pi bk_F^2} \left(\tanh \left(1 + \frac{\epsilon_h}{2T} \right) \right) + \frac{1}{8T \cosh^2 \frac{\epsilon_h}{2T}} \right] \quad (\text{S21})$$

We see that $B_h < 0$. We use this in the main text. The densities around electron pockets are

$$\begin{aligned} (n_{xz}^Y + n_{yz}^X) &= \int \frac{d^2k}{(2\pi)^2} [\cos^2 \phi_Y n_F(\epsilon_Y) + \cos^2 \phi_X n_F(\epsilon_X)] \\ &= \int \frac{d^2k}{(2\pi)^2} [A^2(1 + \beta\Gamma_e)^2 \sin^2 \theta_Y n_F(\epsilon_Y^{nem}) + A^2(1 - \beta\Gamma_e)^2 \sin^2 \theta_X n_F(\epsilon_X^{nem})] \\ &\approx A^2 \Gamma_e^2 \int \frac{d^2k}{(2\pi)^2} \sin^2 \theta \left[2f_Y^{(2)}(k) n'_F(\epsilon_Y^{tet}) + \frac{1}{4} f_Y^2(k) n''_F(\epsilon_Y^{tet}) + \beta f_Y(k) n'_F(\epsilon_Y^{tet}) \right] + (1 + \beta^2 \Gamma_e^2) n_{tet}^{X,Y} \quad (\text{S22}) \end{aligned}$$

In this formula, we used the symmetry between the expressions for the densities at X and Y for $\Gamma_e = 0$ and expanded to second order in Γ_e . We defined f_Y and $f_Y^{(2)}$ by writing $\epsilon_Y^{nem} = \epsilon_Y^{tet} + \Gamma_e/2 f_Y(k) + \Gamma_e^2 f_Y^{(2)}(k)$, where f_Y is given below Eq. (S14), and $f_Y^{(2)} = 2v^2 k_x^2 / \sqrt{(C_1^Y - C_2^Y)^2 + 8v^2 k_x^2}$. We then define $(n_{xz}^Y + n_{yz}^X) = n_{tet}^{X,Y} + B_e \Gamma_e^2$ and compute B_e numerically using the parameters for FeSe from Ref. [17]). We find $B_e < 0$ and $|B_e| < |B_h|$. We use this in the main text.

As we said in the main text, this calculation is not fully self-consistent because we evaluated the "source" term by keeping the terms linear in Γ_h and Γ_e in the orbital Hamiltonian and expanding the densities to order $\Gamma_{h,e}^2$. For a full self-consistent calculation, we should have included also terms of order $\Gamma_{h,e}^2$ into the orbital Hamiltonian, expanded to order $\Gamma_{e,h}^2$ and then solved self-consistently for the prefactor of the Γ_e^2 term near the electron pockets. However, the Γ_e^2 term only appears because of the source term. The prefactor is then proportional to the source term and has the same sign. This is what we used in the main text.

-
- [1] Ying Ran, Fa Wang, Hui Zhai, Ashvin Vishwanath, Dung-Hai Lee, Phys. Rev. B **79**, 014505 (2009).
- [2] S. Graser, T. A. Maier, P. J. Hirschfeld, and D. J. Scalapino, New J. Phys. **11**, 025016 (2009).
- [3] Naoya Arakawa, Masao Ogata, J. Phys. Soc. Jpn. **80**, 074704 (2011)
- [4] A. V. Chubukov, M. Khodas, R. M. Fernandes, Phys. Rev. X **6**, 041045 (2016).
- [5] R. M. Fernandes and A. V. Chubukov, Rep. Prog. Phys. **80**, 014503 (2017).
- [6] see e.g., Anna E. Böhmer, Andreas Kreisel, Journal of Physics: Condensed Matter **30**, 023001 (2017) and references therein.
- [7] K. Matsuura, Y. Mizukami, Y. Arai, Y. Sugimura, N. Maejima, A. Machida, T. Watanuki, T. Fukuda, T. Yajima, Z. Hiroi, K. Y. Yip, Y. C. Chan, Q. Niu, S. Hosoi, K. Ishida, K. Mukasa, S. Kasahara, J.-G. Cheng, S. K. Goh, Y. Matsuda, Y. Uwatoko, and T. Shibauchi, Nature Communications, **8** 1143 (2017).
- [8] P. O. Sprau, A. Kostin, A. Kreisel, A. E. Böhmer, V. Taufour, P. C. Canfield, S. Mukherjee, P. J. Hirschfeld, B. M. Andersen, and J. C. Seamus Davis, Science **357**, 6346 (2017).
- [9] H. C. Xu, X. Niu, D. F. Xu, J. Jiang, Q. Yao, Q. Y. Chen, Q. Song, M. Abdel-Hafiez, D. A. Chareev, A. N. Vasiliev, Q. S. Wang, H. L. Wo, J. Zhao, R. Peng, and D. L. Feng, Phys. Rev. Lett. **117**, 157003 (2016)
- T. Hashimoto, Y. Ota, H. Q. Yamamoto, Y. Suzuki, T. Shimojima, S. Watanabe, C. Chen, S. Kasahara, Y. Matsuda, T. Shibauchi, K. Okazaki, and S. Shin, Nat. Comm. **9**, 282 (2018);
- [10] M. D. Watson, A. A. Haghighirad, L. C. Rhodes, M. Hoesch, T. K. Kim, New J. Phys. **19**, 103021 (2017)
- [11] Y. Suzuki, T. Shimojima, T. Sonobe, A. Nakamura, M. Sakano, H. Tsuji, J. Omachi, K. Yoshioka, M. Kuwata-Gonokami, T. Watashige, R. Kobayashi, S. Kasahara, T. Shibauchi, Y. Matsuda, Y. Yamakawa, H. Kontani, and K. Ishizaka, Phys. Rev. B **92**, 205117 (2015).
- [12] Xingjiang Zhou, private communication
- [13] A. Fedorov, et al., Scientific Reports **6**, 36834(2016).
- [14] A. Coldea and M. Watson, Annual Review of Condensed Matter Physics **9**, 125 (2018).
- [15] In some earlier studies, see e.g., Ref. [21] a larger magnitude of $\Gamma_e \sim 50meV$ has been reported. The authors of later studies argued [10, 13, 14] that $50meV$ is the difference between the energies of d_{xz}/d_{yz} and d_{xy} orbitals.

- [16] Y. S. Kushnirenko, A. V. Fedorov, E. Haubold, S. Thirupathiah, T. Wolf, S. Aswartham, I. Morozov, T. K. Kim, B. Buchner, and S. V. Borisenko, arXiv:1802.08668.
- [17] J. Kang, R.M. Fernandes, and A.V. Chubukov, arXiv:1802.01048.
- [18] A.V. Chubukov, *Annul. Rev. Cond. Mat. Phys.* **3**, 13.1 (2012).
- [19] Fa Wang, Hui Zhai, Ying Ran, Ashvin Vishwanath, Dung-Hai Lee, *Physical Review Letters*, **102**, 047005 (2009); Christian Platt, Werner Hanke, Ronny Thomale, *Advances in Physics* **62**, 453-562 (2013).
- [20] S. Onari, Y. Yamakawa, and H. Kontani, *Phys. Rev. Lett.* **116**, 227001 (2016).
- [21] L. Fanfarillo, J. Mansart, P. Toulemonde, H. Cercellier, P. Le Fevre, F. Bertran, B. Valenzuela, L. Benfatto, V. Brouet, *Phys. Rev. B* **94**, 155138 (2016)
- [22] L. Ortenzi, E. Cappelluti, L. Benfatto and L. Pietronero, *Phys. Rev. Lett.* **103**, 046404 (2009).
- [23] R. M. Fernandes and O. Vafek, *Phys. Rev. B* **90**, 214514(2014)
- [24] V. Cvetkovic and O. Vafek, *Phys. Rev. B* **88**, 134510 (2013).
- [25] R.-Q. Xing, L. Classen, M. Khodas, A. V. Chubukov, *Phys. Rev. B* **95**, 085108 (2017); L. Classen, R.-Q. Xing, M. Khodas, A. V. Chubukov, *Phys. Rev. Lett.* **118**, 037001 (2017).
- [26] In principle, the r.h.s. of Eq. (1) also contains the term $n_{xy}^Y - n_{xy}^X$ as this difference has a piece linear in Γ_e . However this term turns out to be numerically smaller than $n_{xz}^Y - n_{yz}^X$ already at a bare level and we neglect it. Another reason to neglect the contribution from d_{xy} orbital is that for $U > U'$, interactions involving fermions from d_{xy} orbital flow under pRG to progressively smaller values than the ones involving fermions from d_{xz}/d_{yz} orbital. The smallness of the interactions involving d_{xy} orbital also follows from other treatments [Z. P. Yin, K. Haule, G. Kotliar, *Nature Materials* **10**, 932 (2011); L. de' Medici, G. Giovannetti, M. Capone, *Phys. Rev. Lett.* **112**, 177001 (2014); E. Bascones, B. Valenzuela, and M. J. Calderon, *Phys. Rev. B* **86**, 174508 (2012); L. Fanfarillo, G. Giovannetti, M. Capone, E. Bascones, *Phys. Rev. B* **95**, 144511 (2017)].
- [27] See Supplementary Material
- [28] In principle, one has to distinguish between interactions on hole and electron pockets for U_a . However, they differ only by a factor [25]. To simplify the presentation, in the main text we set U_a to be equal on hole and electron pockets. We discuss a generic case in [27].
- [29] The authors of [20] found that the attraction in d^{+-} channel holds also for $U_0 > 0$ (H. Kontani, private communication).